

## Supporting information

### **Near-infrared driven N<sub>2</sub> fixation on ZnO-MXene (Ti<sub>3</sub>C<sub>2</sub>) heterostructures through pyroelectric catalysis**

Chunzheng Wu <sup>a</sup>, Jingyuan Lin <sup>b,c</sup>, Zhuojiong Xie <sup>c</sup>, Xuan Kai <sup>c</sup>, Xiao Yu <sup>c</sup>, Zhenyu Yan <sup>c</sup>, Jinwei Fang <sup>c</sup>, Shanliang Chen <sup>b</sup>, Jianzhong Guo <sup>a\*</sup>, Wei Wang <sup>c\*</sup>, Fengping Peng <sup>c\*</sup>

<sup>a</sup> *College of Chemistry and Materials Engineering, Zhejiang A&F University, Hangzhou 311300, P. R. China.*

<sup>b</sup> *Institute of Micro/Nano Materials and Devices, Ningbo University of Technology, Ningbo 315211, P. R. China.*

<sup>c</sup> *Institute of Advanced Materials and Flexible Electronics (IAMFE), School of Chemistry and Materials Science, School of Environmental Science and Engineering, Changwang School of Honors, Nanjing University of Information Science & Technology, Nanjing 210044, P. R. China.*

\*Corresponding authors: guojianzhong@zafu.edu.cn (J. Guo), wwang@nuist.edu.cn (W. Wang), pengfengping@nuist.edu.cn (F. Peng)

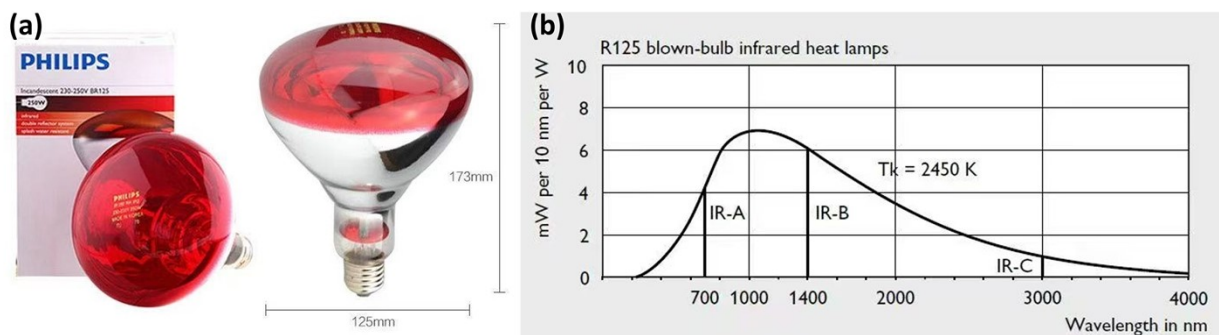


**Figure S1.** (a) a photograph and (b) the spectrum of the R125 blown-bulb infrared heat lamp.

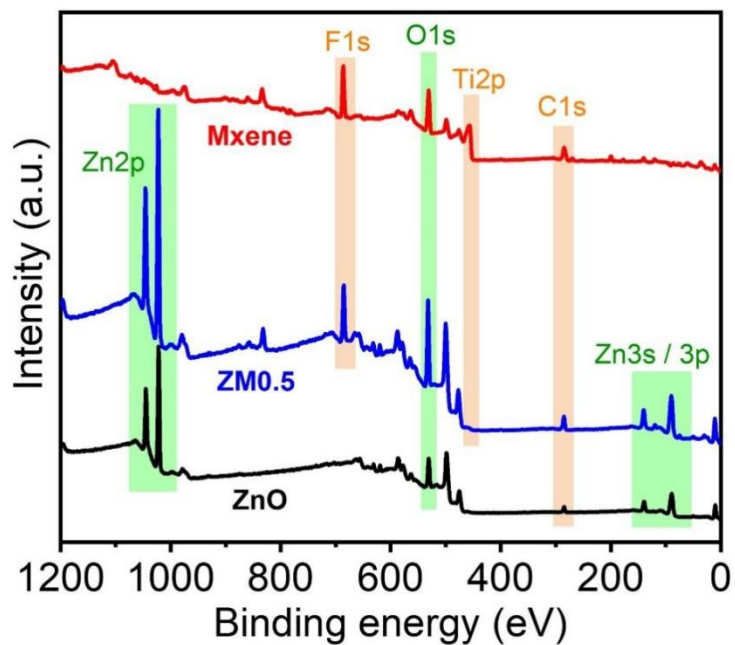


**Figure S2.** XPS survey spectra of ZnO, Mxene and ZM0.5.

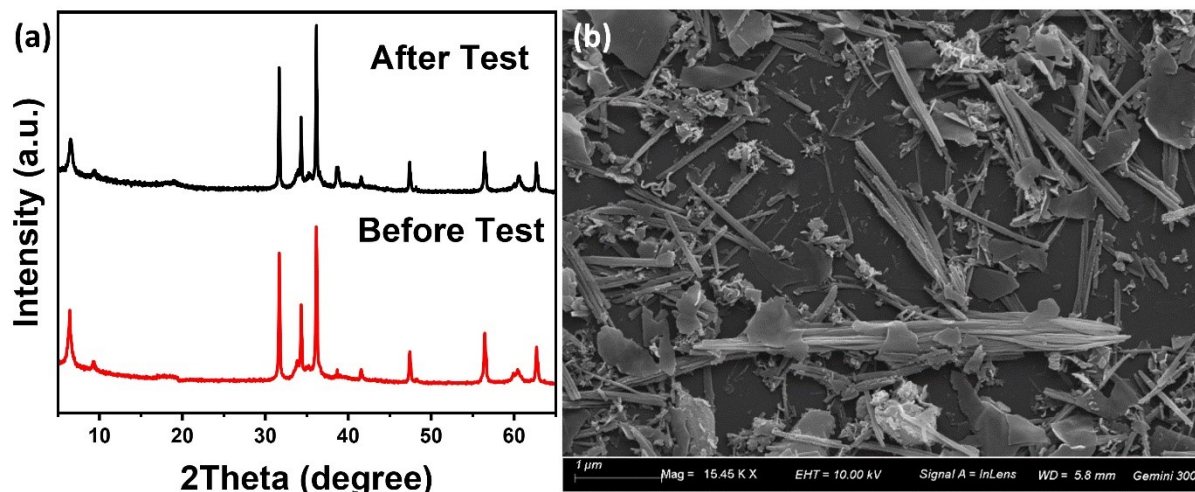


**Figure S3.** (a) XRD patterns of ZM0.5 before and after the catalytic tests. (b) SEM image of ZM0.5 after the catalytic tests.

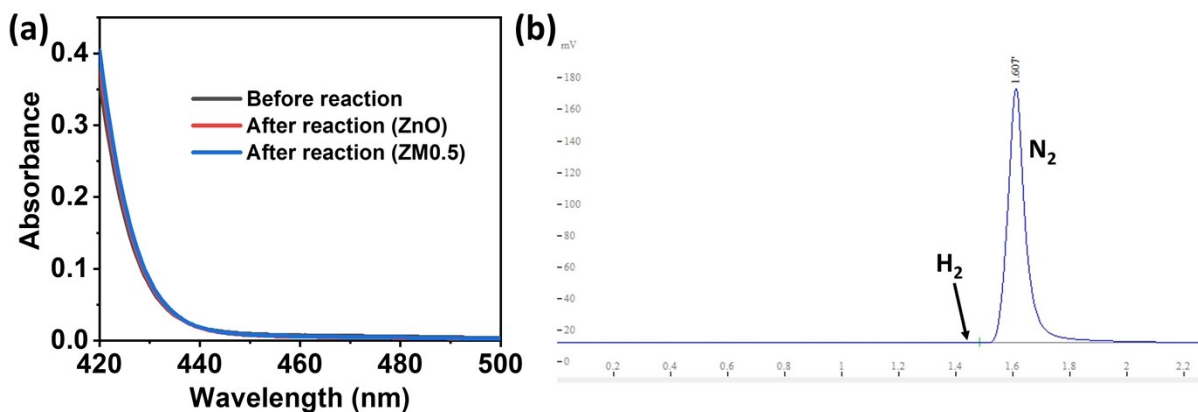


**Figure S4.** Presents the detection results for the reaction products from ZM0.5 after 5 hours. Panel (a) shows the UV-Vis absorption spectra recorded to detect the  $N_2H_4$  product using the  $p-C_9H_{11}NO$  indicator. Panel (b) illustrates the detection of the  $H_2$  product using gas chromatography equipped with a thermal conductivity detector (TCD). In both cases, no product was detected.

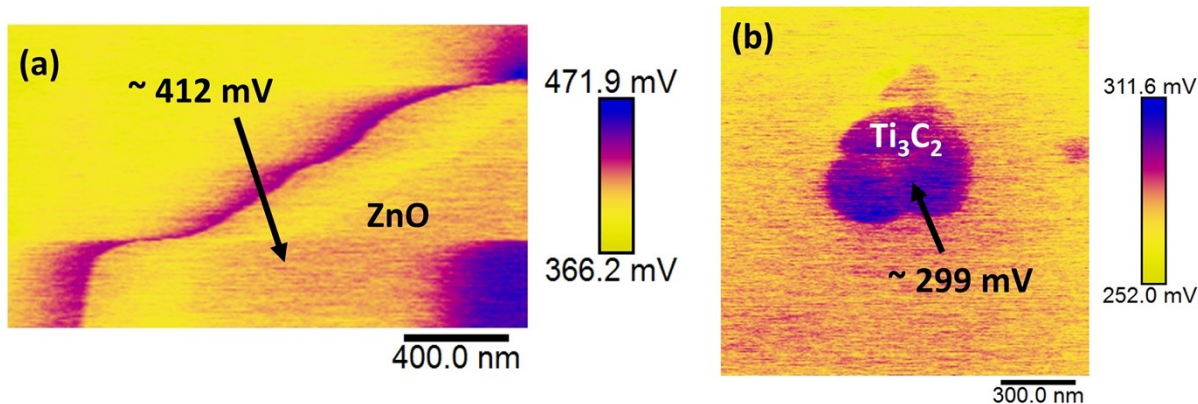


**Figure S5.** KPFM images of (a) ZnO and (b)  $\text{Ti}_3\text{C}_2$  MXene and the corresponding potentials on their surface ( $V_{\text{CPD}}$ ). The work functions difference were calculated as follow:  $e \cdot V_{\text{CPD}} = E_{\text{tip}} - E_{\text{sample}}$ . The work function of the tip ( $E_{\text{tip}}$ ) was - 4.6 eV. So the work functions of ZnO and  $\text{Ti}_3\text{C}_2$  were calculated to be 4.19 eV and 4.31 eV, respectively.

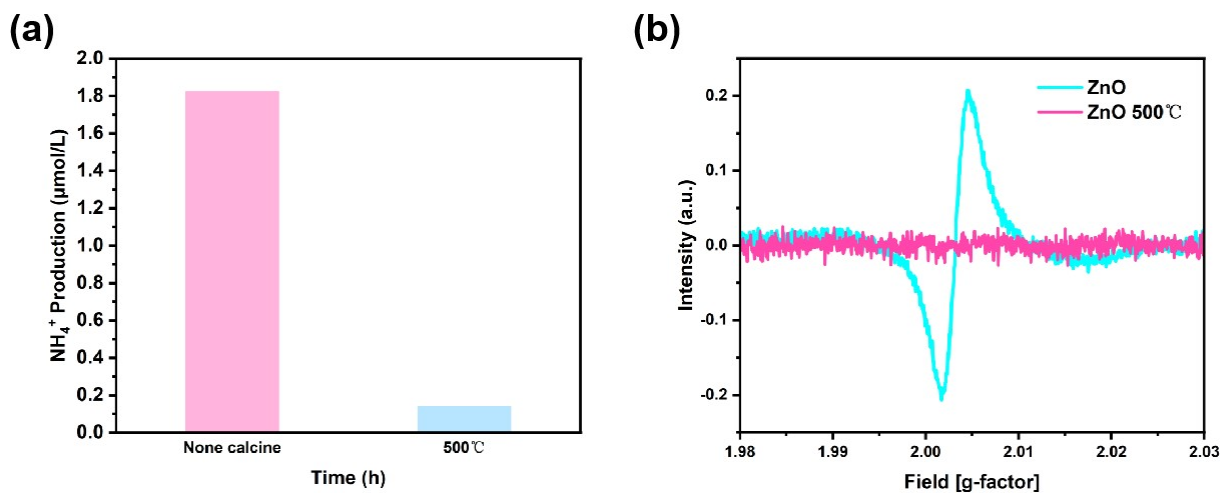


**Figure S6.** (a)  $\text{NH}_4^+$  production of the pristine ZnO and the pre-calcined ZnO to fill its oxygen vacancies; (b) ESR spectroscopy of ZnO before and after a calcination treatment in air. The ESR signal at approximately  $g=2.004$  represents the oxygen vacancy defects on ZnO.

The above experiment confirmed the essential role of the oxygen vacancies on ZnO for the  $\text{N}_2$  fixation reaction. The calcination treatment at 500 °C in air was to refill the oxygen vacancies. It resulted in a dramatic decline of the ammonia production, meaning that the oxygen vacancies on the pristine ZnO contributed to the  $\text{N}_2$  fixation reaction.

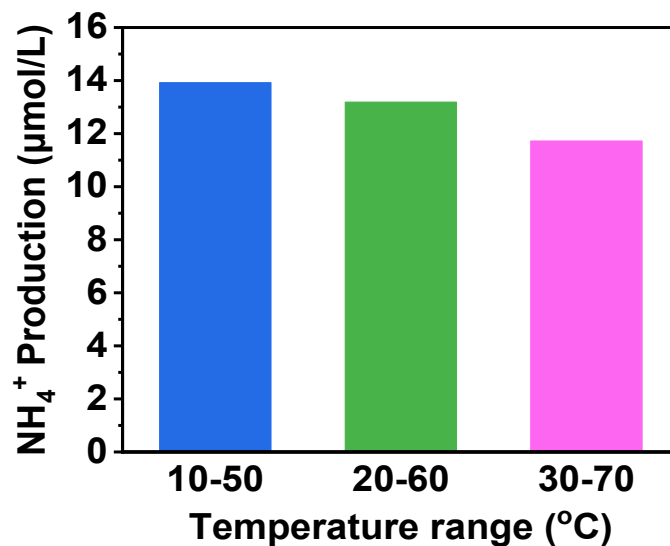


**Figure S7.** ammonia production under different ranges of temperature fluctuation.

**Figure S7** shows the N<sub>2</sub> fixation activity of ZM0.5 at three different temperature ranges. Even with the same fluctuation width (i.e., 40 °C), the fluctuation at higher temperature (i.e., closer to the T<sub>C</sub> of ZnO) does not favor the generation of pyro electrons and holes, thus the catalytic reaction.